ACTUATED TRANSITION IN LP TURBINE LAMINAR SEPARATION – AN EXPERIMENTAL APPROACH

J. Baumann, Institut für Luftfahrtantriebe, Universität Stuttgart
T. Ries, Institut für Luftfahrtantriebe, Universität Stuttgart
M. Rose, Institut für Luftfahrtantriebe, Universität Stuttgart
S. Staudacher, Institut für Luftfahrtantriebe, Universität Stuttgart
I. Raab, MTU Aero Engines GmbH, München

Abstract

Requirements in cost and weight reduction of aircraft engines have led to new design concepts for its components. The reduction of blade counts in the LP turbine is one possibility to cut down weight and therewith costs. While the number of blades per stage decreases, the lift coefficient raises. At low Reynolds numbers the laminar boundary layer on the suction side of high lift LP turbine blades tends to separate and therewith cause losses in turbine performance. For being able to keep these losses limited, in recent years the control of laminar separation bubbles has been subject of many studies.
A project is underway at the Universität Stuttgart to study a possible technique suppressing laminar separation at low Reynolds numbers about 50,000 using actuated transition. In contrast to concepts of steady or pulsed vortex generating jets, no bleed air has to be used as the actuation is done by the momentum from jets of small amplitude. This paper reports about the experimental setup for this study. First results from PIV and hot wire measurements are presented. In addition results from numerical and experimental simulations of fluidic oscillators which are capable to provide the required frequencies at a size which would fit into an LP turbine are shown.

INTRODUCTION

In modern engine design the trend is, in addition to increases in the overall engine efficiency, to reduce the weight and complexity of its components [1]. Therefore stage numbers and blade numbers of Low Pressure Turbines (LPT) are reduced which leads to a reduction of row solidity. At the same time the bypass ratio is increased which means LP turbines are to drive larger fans at lower fan speeds. Due to low Reynolds numbers of about 50,000 in small, high flying business jets or micro gas turbines as used in Unmanned Aerial Vehicles, the laminar boundary layer in those LP turbines can separate. Laminar separation causes reduction in turbine and therewith overall engine performance. That is why laminar separation bubbles (LSB) should be avoided. Many investigations on separation control have been published. These investigations can be distinguished from passive and active flow control. Passive flow control devices, such as turbulence trips or vortex generators cannot adapt themselves to changing operation conditions. This may negatively affect the performance under off-design conditions. Active separation control such as vortex generating jets (VGJ) was investigated amongst others by Schumann [11], Volino [13], Gross and Fasel [4], Rivir et al. [10] and Bons et al. [2]. The synthetic jets are used to form streamwise vortices which transport fluid of high kinetic energy into the separation bubble to minimize or even eliminate it. They can be either steady blowing or pulsed VGJs whereas the latter have been found by Bons et al. [3] to be more effective. In addition to that Stieger and Hodson [12] found out that periodically appearing and disappearing separation bubbles exert less dissipation loss than fully turbulent boundary layers. This leads to the thesis that active separation control in LP turbines is capable of reducing dissipation losses.
In the present study small disturbances with ideally zero net mass flow of distinct frequencies and small amplitude are considered. These disturbances accelerate the laminar turbulent transition process whereby earlier transition leads to a reduced separation. This effect has been investigated by Rist and Augustin [9] and Ricci et al. [6] whereas the latter study was about the boundary layer on wings.
For this work the combination of PIV and hot wire as well as hot film measurements in a low-speed wind tunnel along with DNS-Calculations of this flow will give a fundamental understanding of the processes leading to laminar-turbulent transition in a disturbed low pressure turbine. The conditions of the LPT are simulated in a wind tunnel by a profile on the opposite wall of a flat plate. An experimental setup using a

profile on the opposite wall has been successfully used before by Lang [5].
In this study the profile produces a pressure distribution similar to the distribution in an LPT. A separation bubble forms on the flat plate which is to be influenced by disturbances, small in amplitude and of a certain frequency, brought in shortly before the separation bubble. Small existing disturbances are therewith amplified, leading finally to transition and a more stable boundary layer. Through this process the separation bubble gets smaller without need of a high air mass-flow as for steady blowing actuation.
The experiments are still in an early state. That is why this paper reports about the experimental setup and gives some preliminary results

NOMENCLATURE

A	[m²]	area
c_p	[-]	pressure coefficient
d	[m]	diameter
H_{12}	[-]	shape parameter
f	[Hz]	frequency
k	[-]	scaling factor for orifice plate value calculations
M	[-]	Mach number
p	[Pa]	pressure
R	[J/kgK]	universal gas constant
Re	[-]	Reynolds number
s_c	[m]	profile length
T	[K]	temperature
T_u	[-]	turbulence level
U_∞	[m/s]	free stream velocity
u, v, w	[m/s]	velocity components in x, y and z direction
x	[m]	streamwise coordinate
y	[m]	wall-normal corrdinate
z	[m]	spanwise coordinate

Symbols

δ_1	[m]	displacement thickness
δ_2	[m]	momentum thickness
η	[kg/ms]	dynamic viscosity
κ	[-]	adiabatic exponent
ρ	[kg/m³]	density

Indices

*	effective value
crit	critical value
in	inlet
n	nozzle
out	outlet

Abbreviations

CFD	Computer Fluid Dynamics
FFT	Fast Fourier Transformation
LPT	Low Pressure Turbine
LSB	Laminar Separation Bubble
VGJ	Vortex Generating Jet

1. CONCEPT OF STUDIES

The experimental simulation is of a LP turbine blade suction side at low Reynolds numbers using a simple geometry and assuring Reynolds number similarity. The Reynolds number Re definition for turbines is:

$$Re = \frac{U_\infty \cdot s_c \cdot \rho}{\eta} \tag{1}$$

It is calculated by the chord length s_c, the main flow velocity U_∞ at the trailing edge, the fluid density ρ and the dynamic viscosity η. The low Mach number flow between two turbine blades is modeled with a flat plate and an opposite contour. CFD calculations were used to design a profile which produces a c_p distribution similar to the one of a T161 blade profile on an opposite flat plate as displayed on the right hand side in Figure 1.

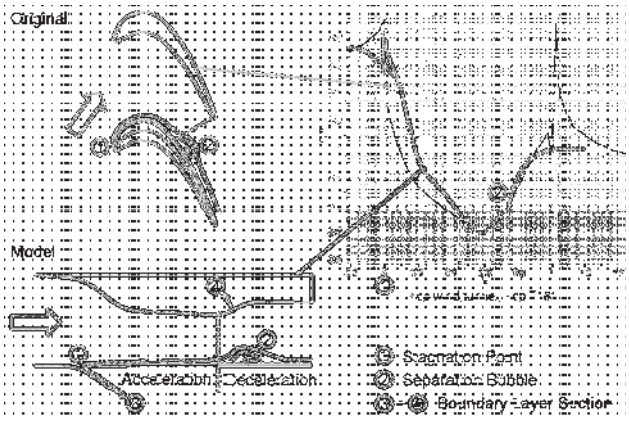

Figure 1: Schematic of concept and diagram of c_p distribution

The local pressure coefficient c_p is defined by the difference of local static pressure and static outlet pressure divided by the difference of total inlet pressure and static outlet pressure according to equation (2):

$$c_p = \frac{p - p_{out}}{p_{tin} - p_{out}} \tag{2}$$

As can be seen in the lower left corner of Figure 1, there are two boundary layer suction devices. The first of them sucks off the boundary layer in such a

manner that a new laminar boundary layer can form. That way a defined stagnation point is formed as at the leading edge of the turbine blade, and in addition any turbulence in the incoming boundary layer is removed. The second bleed is positioned in the deceleration zone on the profiled wall. It sucks the flow to follow the shape of the contour and therewith forces the formation of a separation bubble onto the opposite flat plate.

2. TEST RIG

2.1 Inlet Plenum

The wind tunnel is a suction device driven by a vacuum pump, getting its air from the test hall. The free stream velocity in the test section is very low at about 1m/s. Given that changing environmental conditions were heavily influencing the behavior of the sucked air, an inlet plenum was designed to cut off these influences. Its cross section is ten times as big as those of the test section.

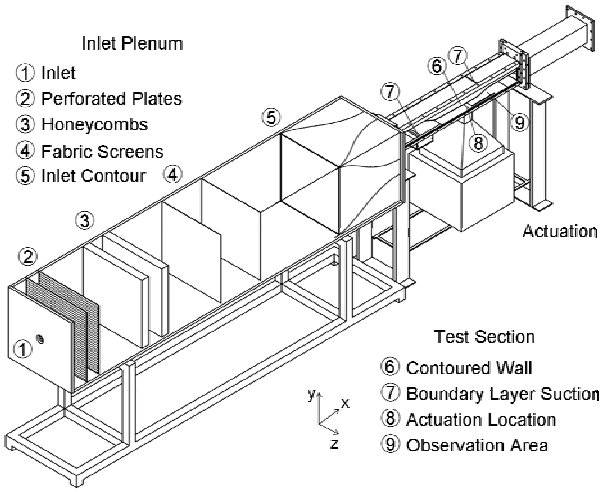

Figure 2: Configuration of the test rig including inlet plenum

The configuration of the test rig and inlet plenum is shown in Figure 2. In contrast to usual laminar flow test rigs the inlet of this plenum is smaller than the cross section of the tunnel (1). The velocity of the sucked air is highly increased by forcing it through the small hole (A_{in}/A_{TS} = 1/10). Therewith influences of environmental disturbances on the flow in the test rig are eliminated. Perforated plates are used as baffles (2) which force the fluid to spread over the whole cross section of the plenum. Round shaped (3mm diameter, 50mm length) honeycombs (3) and fabric screens (4) produce uniformity of the now low speed flow. As a result, strong turbulence produced by the unusual inlet design are damped out and the turbulence level in the inlet of the test section reaches T_u≤0.1%. The contraction from the plenum cross section to those of the test section is done by a sine-cosine passage which enables smooth acceleration of the flow and is unlikely to cause separation.

2.2 Test Section

The test section had to fit an existing wind tunnel setup. Therefore the cross section of the test section was fixed at 100x100mm, the length at 1000mm.
To ensure easy changeability of the modules containing actuation or instrumentation respectively a modular bottom plate was designed as is hinted in Figure 2. Layout of the profiled wall and boundary layer suctions geometries was done by the aid of CFD simulations by Ries and is described in [7]. The profiled wall and one of the side walls are made of Perspex to enable optical access which is needed for PIV measurements that are taken.

2.3 Mass Flow Control

The controlling parameter for the experiments is the Reynolds number according to equation (1) with the length of the profile as chord length s_c.
As this study is about small Reynolds number flow and the test rig is large scale, velocities and mass flows are therefore very small (U_∞≤4m/s). However, the pressure ratio from atmosphere to vacuum pump inlet is very large. Any mass flow control device must be choked, which is why mass flows are set up by orifice plates rather than valves. These orifices are positioned in the downstream pipework and were designed according to DIN EN ISO 5167-2. Under the assumption of critical flow through the orifice plates (M=1.0), the mass flow can be calculated from the effective open orifice area A^*, critical fluid density ρ_{crit} and velocity u_{crit}:

$$(3) \quad \dot{m}^* = A^* \cdot \rho_{crit} \cdot u_{crit} = Ak_A \cdot p_t k_p \cdot \sqrt{\frac{\kappa}{R \cdot T_t k_T}}$$

It depends on the total pressure and total temperature in the test rig. The Reynolds number has to be kept constant to assure similar conditions for different test days.
As already mentioned above, the environmental conditions in the test facility are not constant or controllable. A cone enabling the size of the inlet to be varied was designed as a solution for this problem. If the pressure in the test hall is different to design conditions (Figure 3b), the inlet area can be either reduced or increased by screwing the cone in

(Figure 3c) or out (Figure 3a) respectively. That way the Reynolds number can be kept constant.

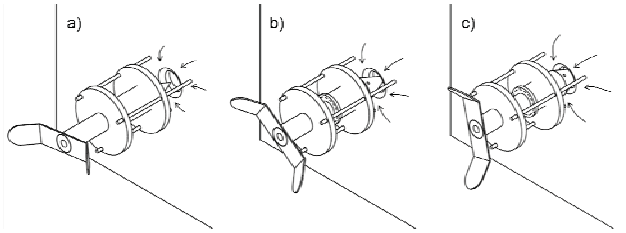

Figure 3: Inlet area variation device in 3 different positions

Changing the inlet area means changing the velocity of the fluid through the inlet. Since the pressure drop scales with the square of the velocity, a defined pressure in the test section can be set up by adjusting the cone depending on the ambient pressure.
The orifices assure that although atmospheric temperature changes vary the mass flow, ratios of bleed to main-stream mass flow stay the same.

2.4 Actuation

The actuation device consists of a loudspeaker box, a plenum, a slot, an amplifier and a computer system as is shown in Figure 4. Via the sound card output of the computer defined frequencies can be generated. They are amplified before being passed to the loudspeaker. The so actuated oscillation of the loudspeakers membrane causes the air in the plenum on top of it to oscillate as well.

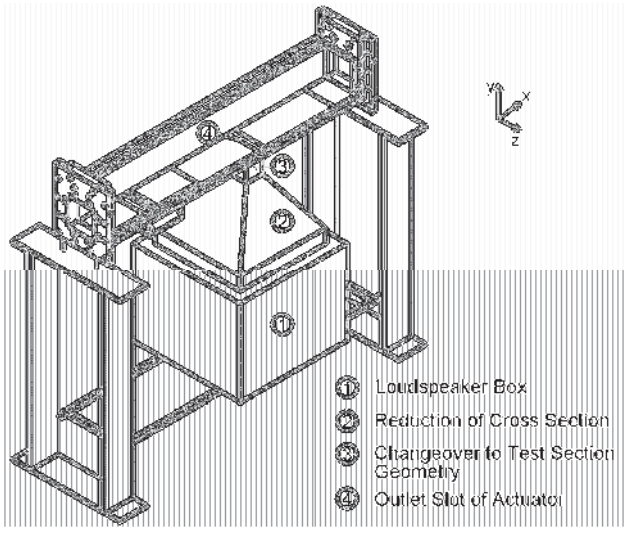

Figure 4: Configuration of actuation device

As is described by Rist and Augustin [9], decelerated flows are sensitive to disturbances of certain frequencies. Once existent, they are amplified exponentially by linear growth mechanisms. These frequencies can be found by the aid of stability analysis. For this study, the frequency analysis was done by Ries [7,8]. As the so defined actuation frequencies are very low at 10-100Hz, depending on the Reynolds number of the flow, the loudspeaker had to be a relatively large bass box (300W, 277mm in diameter).
The slot through which the disturbances are brought into the test rig is shaped rectangular and orthogonal to the wall (width = channel width, gap width = 0,3mm). Its current position is 350mm downstream of the stagnation point. Other actuation positions are to be investigated as well.

3. INSTRUMENTATION

3.1 Constant Temperature Anemometry

For boundary layer traverses and calculation of the turbulence level T_u hot wire measurements are taken. To be able to compare the findings with the numerical simulations, T_u should not exceed 1% which can be regarded as a laminar flow field.
It is calculated, as can be seen in equation 4, from the standard deviations of the measured velocity components u, v and w and the mean free stream velocity U_∞.

$$T_u = \frac{1}{U_\infty} \cdot \sqrt{\frac{1}{3} \cdot \left(\overline{u'^2} + \overline{v'^2} + \overline{w'^2} \right)} \tag{4}$$

(For the past measurements a single-wire hot wire probe was used. Therefore components v and w fall away.)

3.2 Static Pressure Measurements

In addition to those with a hot wire, also static pressure measurements are taken. Static pressure tappings are positioned in important positions in flow direction, i.e. plenum, test section inlet, first boundary layer suction (leading edge), location of expected lowest static pressure (according to CFD simulation), second boundary layer suction and end of profile (trailing edge) as can be seen in Figure 5. With data from these measurements the pressure distribution in the wind tunnel can be compared to simulation results and used as input for new simulations respectively.
Pressure measurements are also used to control the inlet plenum static pressure adjustment by the inlet area variation.

3.3 Temperature Measurements

A temperature probe (thermocouple type K) is positioned in the plenum as data source for viscosity calculation and therewith the Reynolds number. In Figure 5 positions of the temperature probe and hot wire traverses as well as the static pressure tappings are marked.

3.4 Particle Image Velocimetry (PIV)

PIV data are taken with a measurement system from *LaVision*. For most of the investigations two cameras are used to permit (see Figure 5) a wider observation area. The maximum recording frequency is 15Hz whereas the resolution of each camera is 1600x1200px.

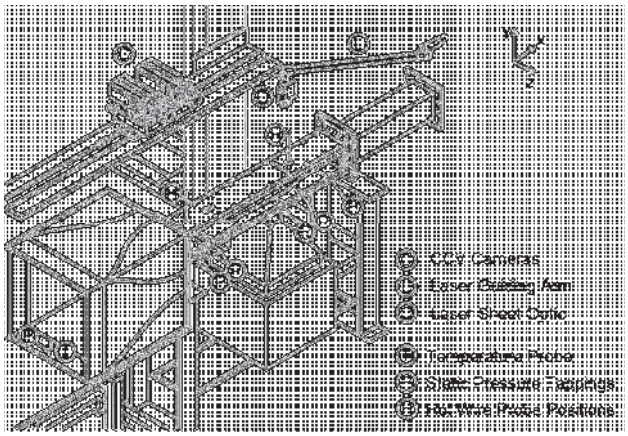

Figure 5: Test rig instrumentation

4. TEST RESULTS

4.1 Inlet Plenum

Hot wire traverses at the inlet of the test section have been made in order to see if the inlet plenum works correctly.

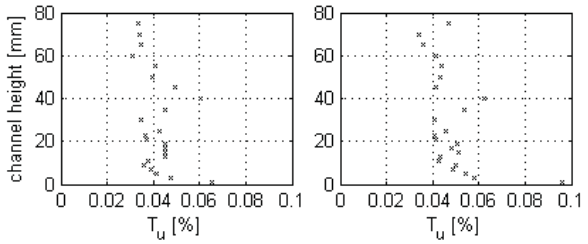

Figure 6: Example turbulence level distributions from hot wire traverses at the test section inlet

In Figure 6 example results for the turbulence level can be seen. It is very low at $T_u \approx 0.05\%$. The flow can therewith be regarded as laminar.

4.2 Test Section

After validating the turbulence level produced by the inlet plenum, an adequate working point for actuation purposes had to be found. The boundary layer suctions had to be adjusted such as a flow field with a reattaching separation bubble was forming. An example flow field without actuation, measured with PIV, is shown in Figure 7.

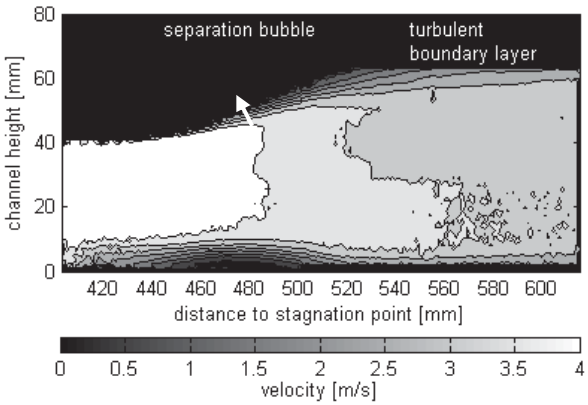

Figure 7: Contour plot from PIV measurement results

The separation bubble that develops in the deceleration area can be identified as the dark bump on the bottom of Figure 7. Due to boundary layer suction on the profiled wall (displayed by a white arrow) this separation does not develop on the profile but on the flat plate opposite to it. The separated flow reattaches again as can be seen on the right hand side of the figure. Because of the deceleration of the tunnel the main velocity decreases (darkens).
In Figure 8 the shape factor related to distance to stagnation point in the wind tunnel is displayed. This value has been calculated from the PIV measurement results according to equation (5).

(5) $$H_{12} = \frac{\delta_1}{\delta_2}$$

Thereby the displacement thickness δ_1 and momentum thickness δ_2 are defined by equations (6) and (7):

(6) $$\delta_1 = \int_0^\infty \left(1 - \frac{u}{U_\infty}\right) dy$$

(7) $$\delta_2 = \int_0^\infty \frac{u}{U_\infty}\left(1 - \frac{u}{U_\infty}\right) dy \,.$$

In non-accelerated or -decelerated flows the shape factor for laminar boundary layers is about 2.54, for turbulent boundary layers 1.3.
In front of the separation zone in Figure 8 the shape factor is of almost turbulent value. The boundary layer could be turbulent, but it is also possible that this is an effect of flow acceleration. This has to be further investigated.
After the separation bubble the shape factor reaches a value of $H_{12} = 1.3$ which indicates a (reattached) turbulent boundary layer.

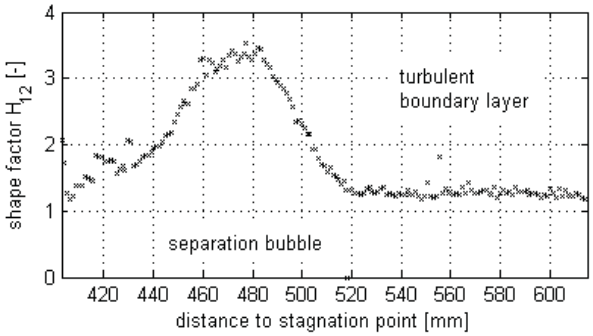

Figure 8: From PIV vector field results calculated shape factor H_{12}

In further investigations this kind of flow field will be studied with actuation.

4.3 Actuation Device

Before the actuation is used in the running test rig, its functionality was checked. Therefore, hot wire measurements have been taken to get information about the actuation jet. The experimental setup is illustrated in Figure 9.

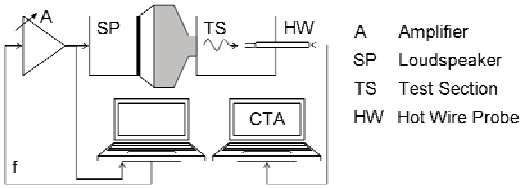

Figure 9: Loudspeaker actuation test setup

The loudspeaker actuation generates a frequent disturbance which was measured by the aid of a hot wire probe. Analyzing the signal of the calibrated probe with Fast Fourier Transformation (FFT), the frequency and related amplitude of the jet can be calculated. In Figure 10 results from a 30Hz actuation can be seen.

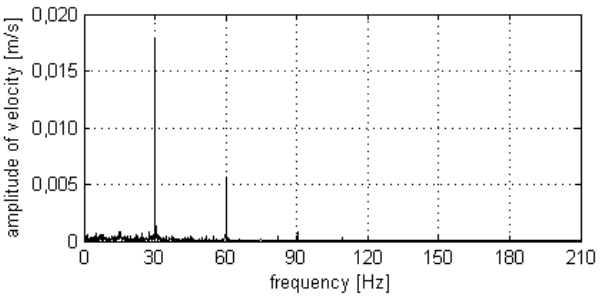

Figure 10: Amplitude of the actuation jet for a nominal frequency of 30Hz measured with a hot wire probe

The hot wire probe was positioned 2mm on top and traversed over the width of the slot. Results from traversing with higher signal amplification are shown in Figure 11.

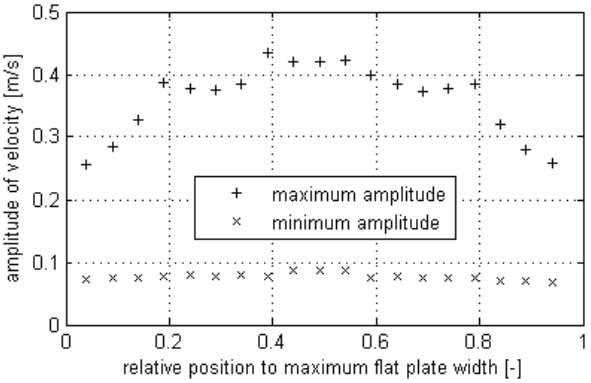

Figure 11: Amplitude distribution of the actuation jet over the actuation slot width

As expected, the amplitude of the jet is not constant over the complete width. But as PIV measurements are taken in the middle plane of the wind tunnel and the actuation amplitude is constant in a range about 8mm left and right of this plane, the actuation setup is satisfactory.

5. TRANSFERABILITY TO TURBOMACHINERY

As already mentioned above, this study focuses on fundamental research. That is why environmental conditions in the test rig are far from turbomachinery reality. This leads to the question how these studies can be used for application in real Low Pressure Turbines. The following two sections will deal with this question.

5.1 Turbulence Level

The very low turbulence level in our studies allows fundamental research. Having no additional sources of disturbances, the actual effect of single frequency actuation can be investigated. Having done this, additional measurements will be taken with a higher turbulence level.
The inlet plenum therefore was designed such as the built in components can be removed. The turbulence level therewith can be increased to 2-4% of free stream velocity which allows better comparison to turbomachinery application.

5.2 Fluidic Oscillator

The actuation setup used in this study is not suitable to turbomachinery application. Frequency actuation devices that produce instability modes in a real turbine need to be small in size and capable of generating the required frequencies at high temperatures. That is why a simple, robust device without moving parts is favorable. Fluidic oscillators can satisfy these boundary conditions.

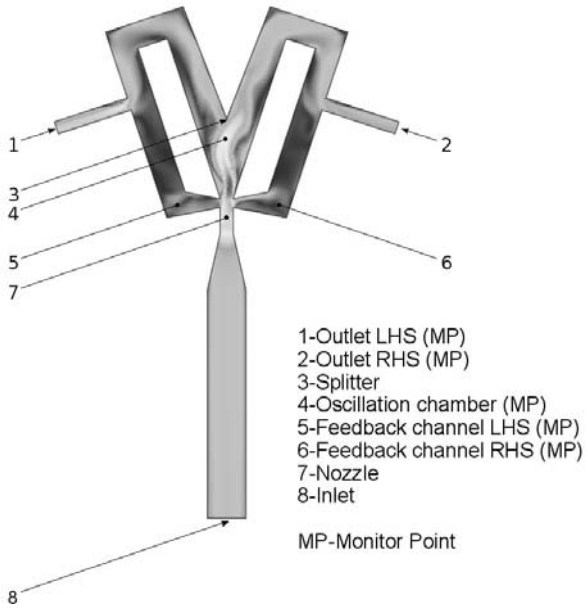

Figure 12: Schematic of the fluidic oscillator taken from Ries [8]

The sectional view of the fluidic oscillator investigated in this study can be seen in Figure 12. By the aid of CFD calculations a 2D geometry was designed that can be extruded to 3D rectangular channels. Therewith efforts in grid generation and the size of the mesh are reduced which leads to a decrease of overall simulation time. Additionally the manufacturing process of the oscillators that are experimentally studied as well is simplified.

5.2.1 Operating Mode

Ries [8] describes the operating mode as follows: “The fluid entering the oscillator at the inlet reaches the nozzle and forms a jet in the oscillation chamber. Due to natural or numerical instabilities in the flow the jet tends to one side of the splitter and travels through the corresponding channel. Most of the fluid leaves the oscillator through the outlet, while a part of the fluid is redirected through the feedback channel, where it reaches the nozzle and forces the jet to switch to the other side of the splitter. This switching is repeated periodically, which results in a pulsed outflow of the fluid at a particular frequency.”

5.2.2 Simulation Results

In Figure 13 the oscillation frequency as a function of Reynolds number is shown. In the corresponding simulations the oscillation frequency was determined with the area-averaged velocity at one of the outlets.

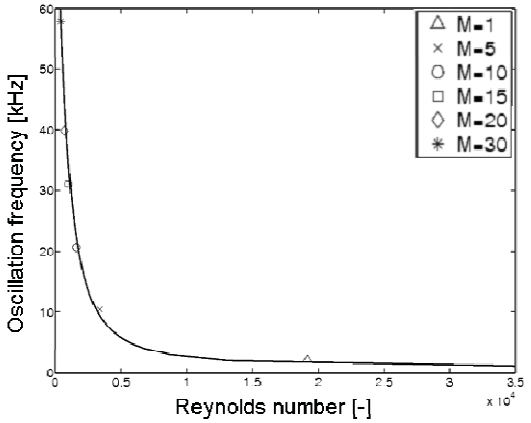

Figure 13: Correlation of Reynolds number and oscillation frequency dependent on oscillator size from CFD simulations, taken from [8]

The Reynolds number (8) is calculated with the area-averaged velocity at the center of the nozzle U_n, its hydraulic diameter d_{hn} and the kinematic viscosity.

$$Re_n = \frac{U_n \cdot d_{hn}}{\nu} \tag{8}$$

Scaling down the whole geometry the Reynolds number variation can be achieved. Individual points for different scaling factors can be approximated by a function of type (9). It may be used to design the oscillator for a special frequency.

$$f = \frac{1}{\ln(Re)}, \quad Re > 1.0 \tag{9}$$

Comparing the oscillation frequencies to the pressure ratio between inlet and outlet, the influence of this pressure ratio can be shown.

Diagrams for two different pressure ratios and the fluid temperature of *T*=298.15K are shown in Figure 14. In the diagram on the left hand side it can be seen that the oscillation frequency gets higher the smaller the oscillator (the bigger the scaling factor) gets. The diagram on the right hand side indicates that a higher ratio of inlet pressure to outlet pressure leads to a higher frequency.

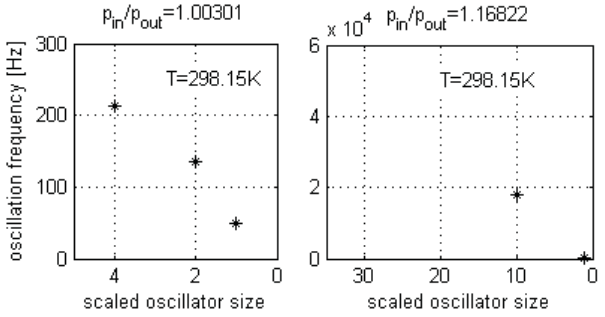

Figure 14: Correlation between oscillator size and oscillation frequency for *T*=289.15K dependent on pressure ratio

As the fluidic oscillator is supposed to be designed for turbomachinery application, additional simulations with LP turbine similar boundary conditions (*T*=776.91K) have been performed. The results of those are displayed in Figure 15.

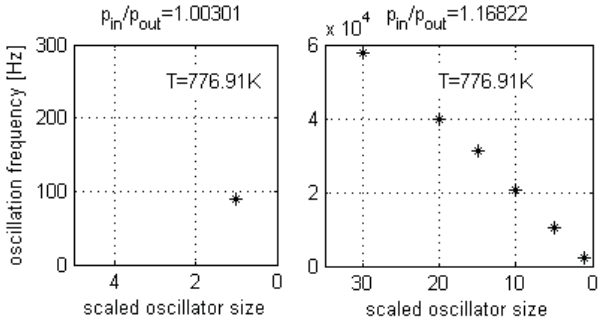

Figure 15: Correlation between oscillator size and oscillation frequency for *T*=776.91K dependent on pressure ratio

On the right hand side diagram a linear correlation between oscillator size and frequency can be seen. The oscillation frequency for the largest oscillator (scaled size 1) is with about 2kHz for the higher pressure ratio twenty times higher than it is with 100Hz for the lower one.
These findings are to be confirmed by the aid of experimental investigations.

5.2.3 Experimental setup

After simulating the fluidic oscillator's performance, experimental investigations are carried out to validate these simulations. Therefore three different sizes of oscillators have been produced. A picture of them is shown in Figure 16. Dependent on the manufacturing process chosen, the smallest scale produced was 15 (on the left in the picture). The oscillator is 30mm long (including the feeding channel) with a nozzle width of 0.33mm. The height of its channels is 0.42mm.

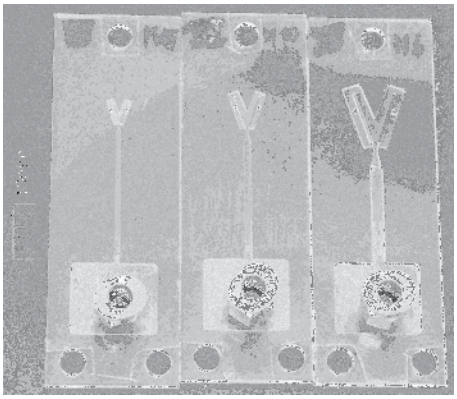

Figure 16: Comparison of three oscillator sizes

In Figure 17 the setup of the experiments including pressure and temperature measurement probes is shown.

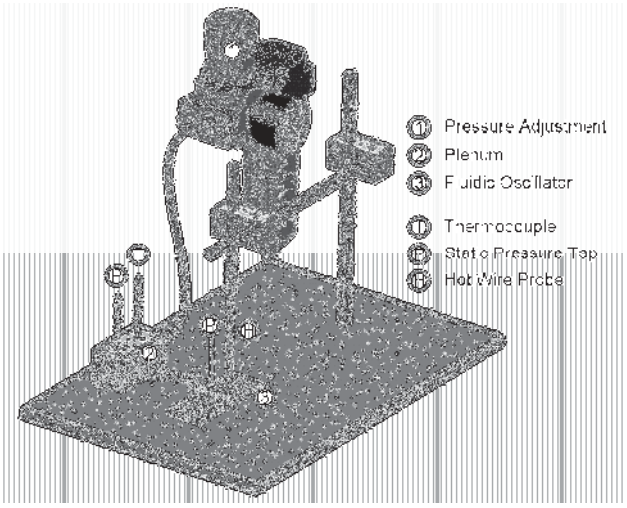

Figure 17: Experimental fluidic oscillator setup

As the driving parameter for the fluidic oscillator is the pressure ratio between inlet and outlet, both pressures have to be measured. The inlet pressure is adjusted by a pressure regulating valve (1).
The outflow of the oscillator is measured with a single hot wire probe. Via FFT analysis of the data the corresponding frequency of the produced jet for each pressure ratio can be calculated.

5.2.4 Experimental Results

Some example results for the three oscillator sizes can be seen in Figure 18. The pressure ratio was varied to see its influence on the oscillation. As has already been showed by numerical simulation, the frequency scales with both: oscillator size and pressure ratio.

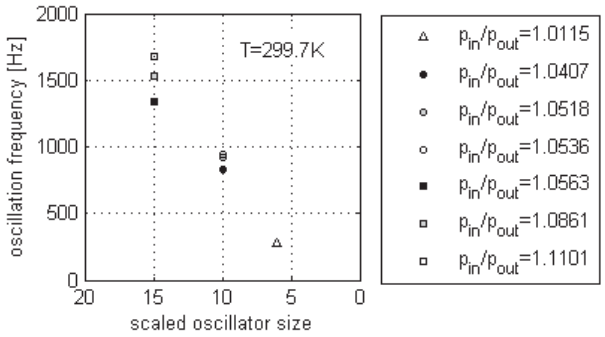

Figure 18: Correlation between oscillator size and frequency dependent on pressure ratio

As the numerical simulations have been performed before the experimental setup and the manufacturing process of the oscillators was defined, pressure ratios and temperatures differ from those of the experiment. To enable comparison of the results from both, additional simulations with boundary conditions from the experiments will be made.

6. CONCLUSIONS AND OUTLOOK

This paper contains the description of the test rig at the Institut für Luftfahrtantriebe at the Universität Stuttgart that is used for investigations on transition actuation by small disturbances (instabilities). A low-Reynolds-number flow field in a rectangular wind tunnel with a c_p distribution similar to the one of an LP turbine is used for the investigations. By the aid of Particle Image Velocimetry and hot wire measurements it was shown that the experimental setup fits the requirements. Also the loudspeaker actuation system was proved to work satisfyingly.

Subject of future investigations will be the influence of the actuation frequency and amplitude as well as their location on the separation bubble.
In addition results from research activities about fluidic oscillators which could be used to excite such disturbances in an LP turbine environment are presented. The oscillation frequency was proved to be driven by pressure ratio between inlet and outlet as well as oscillator size. Further investigations on this relation will be done experimentally as well as by the aid of numerical simulation.

ACKNOWLEDGMENTS

The financial support of VITAL SP6, work package 6.4, task 6.4.3 is acknowledged.

REFERENCES

[1] Ardey, S.; Gier, J.; Hübner, N. (2000), Kostenreduktion durch neue Aerodynamische Konzepte bei Niederdruckturbinen, Deutscher Luft- und Raumfahrtkongress 2000, Jahrbuch 2000 Band I

[2] Bons, J.; Hansen, L.; Clark, J.; Koch, J.; Sondergaard, R. (2005), Designing Low-Pressure Turbine Blades With Integrated Flow Control, ASME Paper No. GT2005-68962

[3] Bons, J.; Reimann, D.; Bloxham, M. (2008), Separated Flow Transition on an LP Turbine Blade With Pulsed Flow Control, Journal of Turbomachinery, 2008, 130, 021014-1-021014-8

[4] Gross, A.; Fasel, H. (2004), Active Control of Separation for Low-Pressure Turbine Blades, AIAA Paper No. AIAA 2004-2203

[5] Lang, M. (2005), Experimentelle Untersuchungen zur Transition in einer laminaren Ablöseblase mit Hilfe der Laser-Doppler-Anemometrie und der Particle Image Velocimetry. Dissertation, Universität Stuttgart, Verlag Dr. Hut, München

[6] Ricci, R.; Montelpare, S.; Silvi, E. (2007), Study of acoustic disturbances effect on laminar separation bubble by IR thermography, Experimental Thermal and Fluid Science, 2007, 31, 349-359

[7] Ries, T.; Baumann, J.; Rose, M.; Staudacher, S. (2009), LP Turbine Laminar Separation Bubble Study: Flat Plate DNS Calculations and Preliminary PIV Data, European Turbomachinery Conference 8, Graz, 2009

[8] Ries, T; Mohr, F.; Baumann, J.; Rose, M.; Rist, U.; Raab, I.; Staudacher, S. (2009), LP Turbine Laminar Separation with Actuated Transition; DNS, Experiment and Fluidic Oscillator CFD, ASME Paper No. GT2009-59600

[9] Rist, U.; Augustin, K. (2005), Control of laminar separation bubbles using instability waves, Proc. ISABE-2005-1041, AIAA Journal 44 (10), October 2006, 2217-2223

[10] Rivir, R. B.; Sondergaard, R.; Bons, J. P; Yurchenko, N. (2004), Control of separation in turbine boundary layers, AIAA Paper No. AIAA 2004-2201

[11] Schumann, T.; Rose, M.; Staudacher, S., Gier, J.; Schroeder, T. (2008), The Effects of Steady Injection on an Ultra High Lift Vane in a LP Turbine, ASME Paper No. GT 2008-50330

[12] Stieger, R. D.; Hodson, H. P. (2003), Unsteady dissipation measurements on a flat plate subject to wake passing, Proc. Instn Mech. Engrs., 2003, 217 Part A, 413-420

[13] Volino, R. (2003), Separation Control on low-pressure turbine airfoils using synthetic vortex generator jets, ASME Paper No. GT2003-38729